

Article

Analysis of the Interaction Damage Mechanism and Treatment Measures for an Underpass Landslide Tunnel: A Case from Southwest China

Wangwang Zhou, Xulin Xu, Xiaoqing Li * and Shiyun Li

School of Civil and Hydraulic Engineering, Huazhong University of Science and Technology, Wuhan 430074, China; civil_zww@163.com (W.Z.)

* Correspondence: xql@mail.hust.edu.cn

Abstract: Previous studies have analyzed the damage of tunnels and slopes as a single entity, ignoring the interaction effect between the tunnels and slopes, which will have an impact on the accuracy of the damage mechanism and the safety of the treatment measures. In this paper, three types of simulation models are established—the natural state, after tunnel excavation, and after reinforcement measures—considering a case study of an underpass landslide tunnel in southwest China. Based on the theory of underpass landslide tunnels and the strength reduction method, the interaction damage mechanism of this underpass landslide tunnel is revealed, and a reasonable treatment plan is proposed. The analysis results show the following: there is an obvious interaction effect between the tunnel collapse and the slope instability; a large number of mudstones common in the surrounding rock of the tunnel have rheological properties, which amplify the influence of the interaction effect of the tunnel through the landslide; and the proposed comprehensive treatment measures of “rescue inside the tunnel cave + tunnel slope treatment” have strong pertinence and effectiveness, and they fundamentally address the tunnel collapse and the slope instability of the tunnel.

Keywords: underpass landslide tunnel; interaction effect; strength reduction method; damage mechanisms; treatment measures



check for updates

Citation: Zhou, W.; Xu, X.; Li, X.; Li, S. Analysis of the Interaction Damage Mechanism and Treatment Measures for an Underpass Landslide Tunnel: A Case from Southwest China. *Sustainability* **2023**, *15*, 11398. <https://doi.org/10.3390/su151411398>

Academic Editors: Fusong Wang, Wenxiu Jiao, Zhilong Cao and Anqi Chen

Received: 4 July 2023
Revised: 18 July 2023
Accepted: 19 July 2023
Published: 22 July 2023



Copyright: © 2023 by the authors. Licensee MDPI, Basel, Switzerland. This article is an open access article distributed under the terms and conditions of the Creative Commons Attribution (CC BY) license (<https://creativecommons.org/licenses/by/4.0/>).

1. Introduction

As one of the important structures in transportation, tunnels have the advantages of shortening the route mileage, improving alignment, saving space, and protecting vegetation, bringing huge social and economic benefits. Geological hazards, such as subsidence and landslides, are often triggered during the construction of highway tunnels in mountainous areas due to human-made excavation and natural disasters [1]. In terms of human causes, the effects of poor drainage systems [2], excessive explosive excavation blasting [3], anchor failure [4,5], and so on bring a great threat to the safety issue. In addition to the damage caused by human-made disturbances that destabilize tunnel slopes, tunnel construction is tested by the geological environment, climate, and natural disasters. The development of unstable rock masses [6,7], tunnel slope inclination [8], rainfall [9–11], earthquakes [12–14], and fires [15–17] all have adversely affected the safety of tunnel construction and normal operation. The effective control of the slope instability damage in tunnels and post-disaster treatment have been the focus of research in the field [18]. Sensors [19,20], optical fibers [21], and other monitoring and measuring methods are usually used to evaluate the deformation characteristics and stability of tunnel slopes, and protection techniques, such as prestressed concrete cylinder pipe [22], pipe jacking [23], and construction optimization [24,25], have been developed. However, the geological conditions of tunnel engineering are complex, and the applicability of protection techniques is not widespread. Therefore, it is necessary to clarify the force pattern and damage mechanism of tunnel landslides to propose reasonable prevention and treatment methods for specific projects. Clarifying the damage

mechanism of tunnel slopes can provide a theoretical reference for the design of tunnel slope engineering and is the key to the design of related management engineering.

To ensure the safety of tunnel construction, many scholars have conducted much research for this purpose. Koçkar et al. [26] used simulation to analyze the stress and deformation at each section of the tunnel by considering the interaction of the support on the surrounding rock. Kong et al. [27] proposed a function to express the deformation mode of the tunnel slope, which can provide a simplified index for the slope deformation. Kaya et al. [28] used kinematics to analyze the stability of the slopes and explored the failure mechanism. Lei et al. [29] established a simulation test system based on a similar theory to analyze the bias and load characteristics for small clearances and shallow burial. Due to the poor geological conditions, severe weathering of the rock, complex topography, and the disturbance of the tunnel construction, the tunnel entrance section is prone to deformation and instability of the tunnel slope, resulting in geological damage, such as landslides and collapses, which are commonplace for tunnel construction accidents. As a result, there is a wealth of research related to the entrance section of tunnels, such as structural damage to the lining of the entrance section [30], risk assessment of the entrance section using neural networks [31], the interaction between the cavern envelope and the lining under seismic action [32], location of seismic weak points in the cavern section [33], the establishment of a three-dimensional dynamic construction model of the cavern section combined with monitoring and measurement to analyze the extent of its deformation [34], the effect of rainfall on the slope stability of the cavern, and the impact of rainfall on the slope stability of the cave entrance section [35]. The results of Hou et al. [36] showed that the combined effect of excavation and rainfall led to damage to the foot of the tunnel slope, which, in turn, led to slope instability as the extent of the damage expanded. The above studies have contributed to the damage mechanism and stability of tunnels and slopes, but they all have studied tunnels and slopes as single entities, ignoring the interaction effect between tunnels and slopes, which has an impact on the accuracy of the damage mechanism and the safety of the treatment measures.

Based on the above analysis, this paper considers a case study of tunnel collapse and slope instability during the construction of a highway tunnel in Southwest China. By combining site investigation, geological exploration, indoor geotechnical testing, and monitoring and measurement, the damage mechanism of the interaction between tunnel collapse and slope instability is analyzed using the strength reduction method and the theory of underpass landslide tunnels. Through a detailed analysis of the damage pattern, a targeted treatment plan of “tunnel cave-in + tunnel slope treatment” is proposed based on simulations and the actual on-site conditions. This plan effectively addresses the issues of tunnel collapse and tunnel slope instability, ensuring the safety of tunnel construction and slope stability. Considering that the tunnel envelope type observed in this case study is prevalent in southwest China, the analysis of the damage mechanism and the proposed treatment measures holds significant research value. The findings of this study can serve as a valuable reference for similar projects, providing insights into the understanding and management of the interaction between tunnel collapse and tunnel slope instability.

2. Project Overview

The proposed highway tunnel is a short, separated over-ridge tunnel with an overall alignment of approximately 310° , and the entrance and exit are both end-wall type, with the left and right tunnel holes entering from the exit end. The left line of the tunnel starts and ends at pile number ZK141 + 875 to ZK142 + 200, with a design length of 325 m. The design elevations of the inlet and outlet roadbeds are 863.534 m and 870.674 m, respectively, with a maximum depth of approximately 76 m (at ZK142 + 020); the right line starts and ends from pile number K141 + 890 to K142 + 180, with a design length of 290 m. The design elevations of the inlet and outlet roadbeds are 863.839 m and 870.674 m, respectively. The design elevations are 863.839 m and 869.719 m, respectively, with a maximum depth of approximately 72 m (at K142 + 010). The natural slope of the mountain is approximately

25–35°, the vegetation on the mountain is more developed, the lower part of the slope is planted with orange trees and other economic forests, and the upper part of the slope is dominated by weeds and orange trees. A schematic representation of the underpass landslide tunnel hazard is shown in Figure 1.

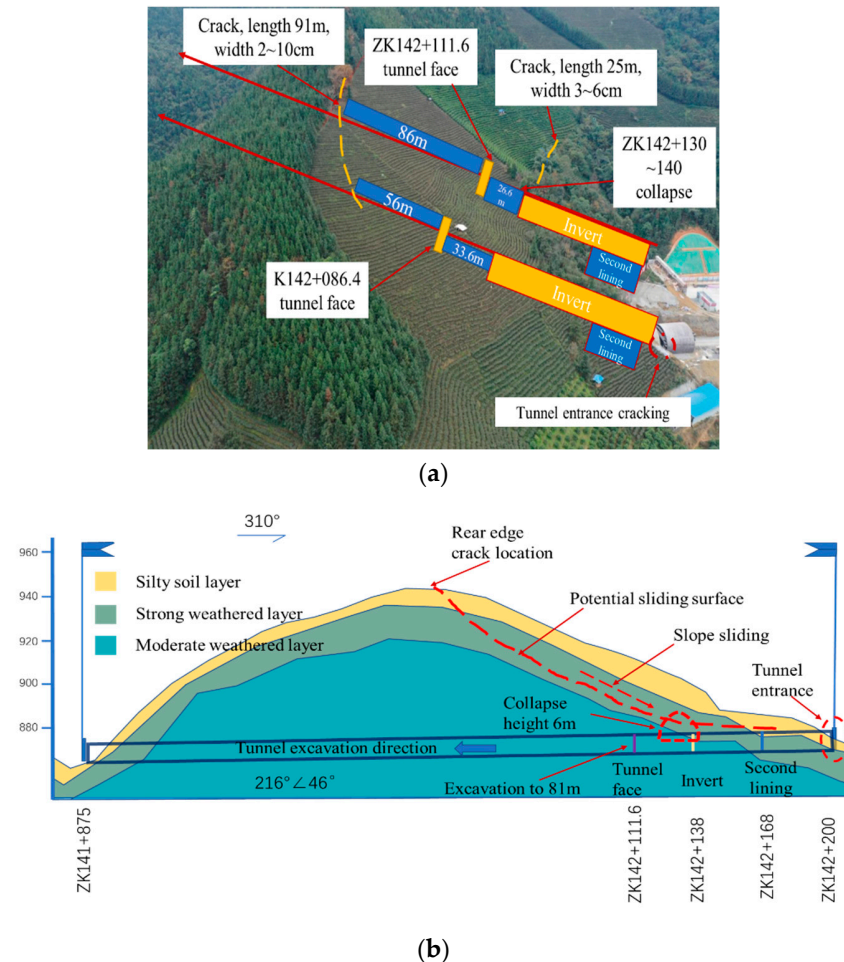


Figure 1. Schematic diagram of the damage to the underpass landslide tunnel. (a) Schematic diagram of the overall damage to the underpass landslide tunnel. (b) Schematic diagram of the damage to the longitudinal section of the underpass landslide tunnel.

2.1. Geological Survey

The tunnel site area does not see active fracture tectonic development affected by regional geological action, and the rock production, joints, and fissures vary greatly. The underlying bedrock in the tunnel area is sandstone with mudstone, mostly in thin and medium laminated formations, and the fissures are mainly weathered fissures with a high density of development. The rock production in the tunnel area is $216^\circ\angle 46^\circ$ (inclined in the slope), and the two sets of joints are J1: $16^\circ\angle 28^\circ$ (4–5 articles/m) and J2: $118^\circ\angle 83^\circ$ (5–6 articles/m). The groundwater is mainly pore water in the Quaternary overburden and bedrock fracture water in the bedrock, and the groundwater at the palm face was not developed during the survey and construction. The stratigraphy of the tunnel slope is composed mainly of the Quaternary residual slope layer and the Middle Triassic Lanmu Formation. The residual slope deposit of the Quaternary system: powdered clay—greyish yellow, hard plastic, mainly clay powder particles, containing a small amount of gravel, medium dry strength, medium toughness, thickness of 0.50–2.40 m. The Middle Triassic Lanmu Formation: the lithology of the site is mainly sandstone interbedded with mudstone, and the mudstone is mainly interbedded or interbedded in the sandstone layer. The mudstone is a muddy structure, extremely soft, easily softened by water, and easily disintegrated

after prolonged exposure to the sun; the sandstone is a silt-like structure, thinly laminated and hard. Depending on the degree of weathering, the rocks can be divided into strongly weathered layers and moderately weathered layers.

A total of 309 slope sections were investigated in a site exploration survey of highway slopes greater than 30 m in height in southwest China, and the damage patterns of the slopes were counted, as shown in Figure 2. The slope sections with circular sliding, parallelogram sliding, wedge sliding, and manual excavation damage accounted for approximately 2%, 33%, 57%, and 8% of the slope sections, respectively. Combined with the comprehensive analysis of the slope investigation where sliding and slumping have occurred on-site, the number of slopes where large-scale parallelogram sliding occurred on-site is relatively small, and more landslides are localized reverse-layer or cut-layer wedge sliding, although reverse-layer or cut-layer working conditions are conducive to slope stability. According to field research, most of the sections in southwest China are Tertiary sandstone slopes, and some of the rock masses are strongly disintegrated, with thicker strongly weathered layers, so wedge sliding occurs more often. The landslides investigated in this study are wedge slides, which are typical in southwest China.

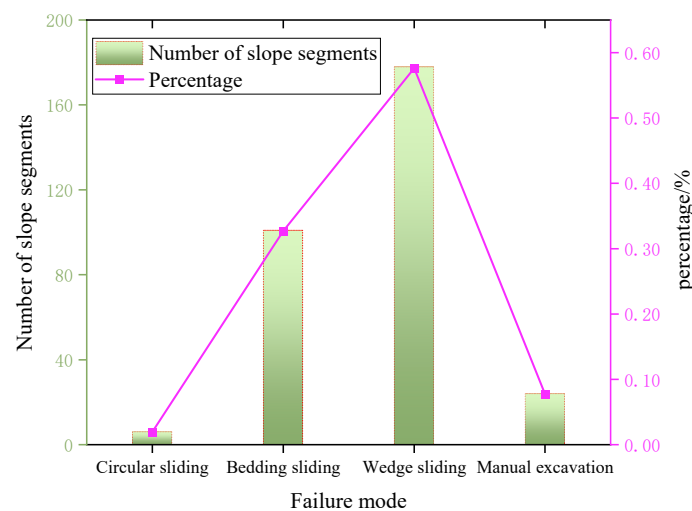


Figure 2. Slope damage pattern.

2.2. Theory of Underpass Landslide Tunnels

A large number of engineering examples show that the relative position of the tunnel and the landslide structural form will have a greater impact on the force deformation and damage mode; therefore, to determine the spatial location of the tunnel and landslide for the study of tunnel–slope interaction, a damage mechanism is essential. In this paper, the tunnel landslide system is a subway landslide tunnel, whose damage is dominated by the deformation of the arch, which is affected by the additional load of the landslide thrust to induce extrusive deformation and cracking. The misplaced platform, the crack width of the cavity section, is large with an extended length; the closer the cavity section deformation is, the more likely it is that a more serious collapse and roofing and other accidents may occur [37,38]. The spatial location of the tunnel through the landslide is shown in Figure 3, and the force pattern is shown in Figure 4. Based on the strength reduction method, the slope safety factor F_s is used as an indicator to evaluate the stability of the slope, and its physical meaning is the ratio of the slip resistance of the soil to the sliding force, where $F_s < 1$ means that the slope has been destabilized and damaged [39]. The maximum disturbance radius R_{pmax} of the tunnel excavation, the maximum additional load max on the lining corresponding to the thickness H_0 , and the minimum safe undercutting distance H_{min} of the tunnel can be calculated according to the following equations [40,41]:

$$R_{pmax} = r_0 e^{(\theta - \rho) \cot(45^\circ + \frac{\phi}{2})} \quad (1)$$

$$H_0 = \sqrt{\frac{3p_i \sin \beta}{2\pi q_{max}}} \quad (2)$$

$$H_{min} = H_0 + R_{pmax} = \sqrt{\frac{3p_i \sin \beta}{2\pi q_{max}}} + r_0 e^{(\theta - \rho) \cot(45^\circ + \frac{\varphi}{2})} \quad (3)$$

where r_0 is the tunnel radius; θ is the friction angle on both sides of the topsoil column; ρ is the initial rupture angle; φ is the internal friction angle of the surrounding rock; and p_i is the landslide thrust.

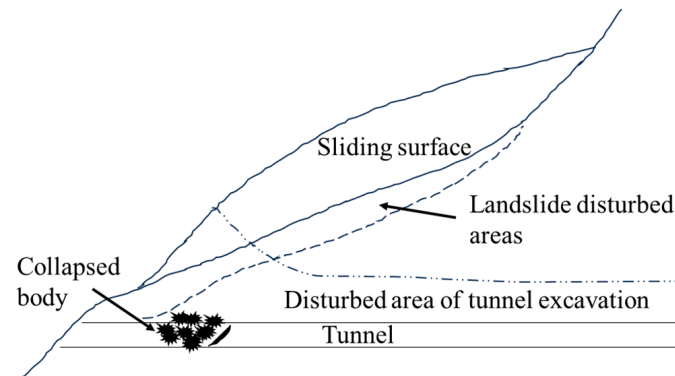


Figure 3. Spatial location relationships.

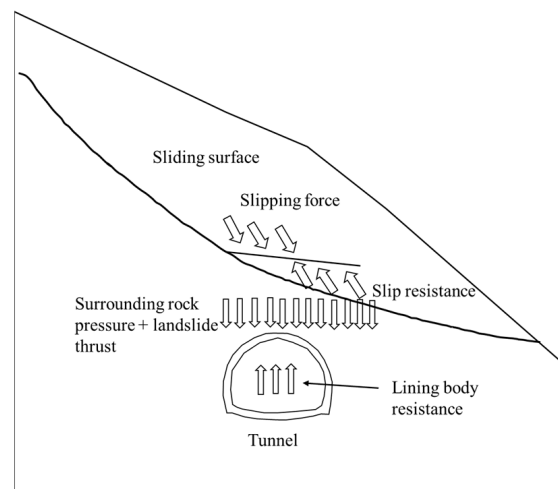


Figure 4. Force pattern.

3. History of the Evolution of Slope Failure in Tunnels

The tunnel was excavated to 88.4 m, the pile number of the palm face of the left hole was ZK142 + 111.6, and the pile number of the left elevation arch was ZK142 + 138. After retrieving the tunnel monitoring and measurement data, the top of the arch of the left hole at ZK142 + 138 settled approximately 1 cm, the top of the arch of the left hole at ZK142 + 118 settled approximately 3 cm, and circumferential cracks appeared in individual piles. After analysis, it is believed that the abnormal deformation in the cave was due to the back-arch and tunnel excavation. The pile number of the palm face of the right cave was K142 + 086.4, the pile number of the right elevation arch was K142 + 120, and there were no abnormalities in the tunnel monitoring and measurement data.

On 16 November 2020, a small collapse occurred at ZK142 + 130–140 in the left cavern of the tunnel, with a volume of approximately 200 m³, forming a 6 m high collapse cavity at the top of the palm face, which extended along the side of the ridge. A photograph of the collapse at the palm face is shown in Figure 5. The lower and middle parts of the palm face are medium-weathered rocks, while the upper part is strongly weathered.

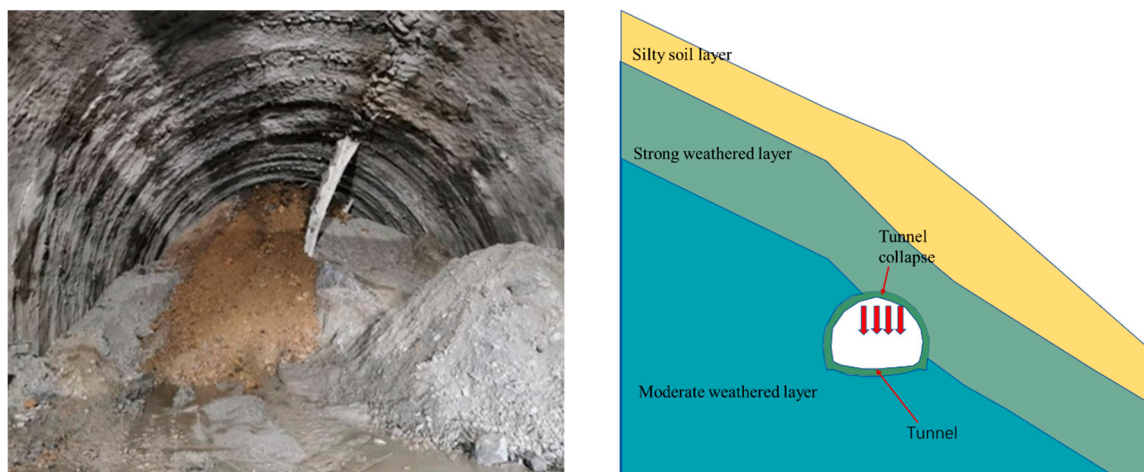


Figure 5. Collapse map of tunnel face.

On 20 December 2020, a crack of approximately 25 m in length and 3–6 cm in width appeared on the left side of the mountain at a location of approximately 45–70 m. The crack was presumed to be caused by the collapse of the left tunnel, as shown in Figure 6.

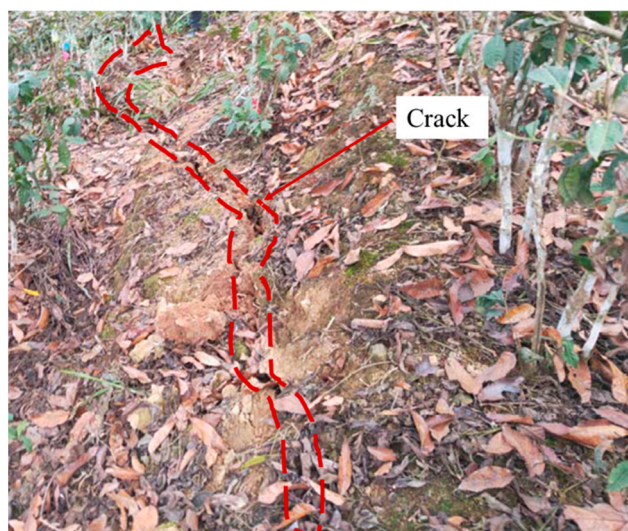


Figure 6. Crack map on the left side of the mountain.

On 30 December 2020, deformation and cracking damage occurred on the elevation slope of the back edge of the tunnel cavity, which was found after an investigation with all parties. The crack was approximately 91 m long and varied in width from 2 to 10 cm. The crack extended along the ridge against the side of the large pile number, 86 m from the left cave and 56 m from the right cave. The side of the small pile number of the crack was a temporary ditch excavated by the villagers, and the ditch was long in scope, extending from the top of the hill to the foot of the hill. The back edge elevation slope of the site is shown in Figure 7.

After the instability of the elevation slope, the site investigation and survey found that cracks appeared in the initial support at the top and waist of the arch of the left hole ZK142 + 130~ZK142 + 140, and cracks appeared in the top and waist of the arch of the right hole K142 + 115. The second lining section of the left cavern was poured in November 2020, and according to the on-site investigation, the second lining section was cracked and damaged, and there was the phenomenon of flaking of the initial support. The cracking of the right lining is shown in Figure 8, and the cracking of the left lining is shown in Figure 9.

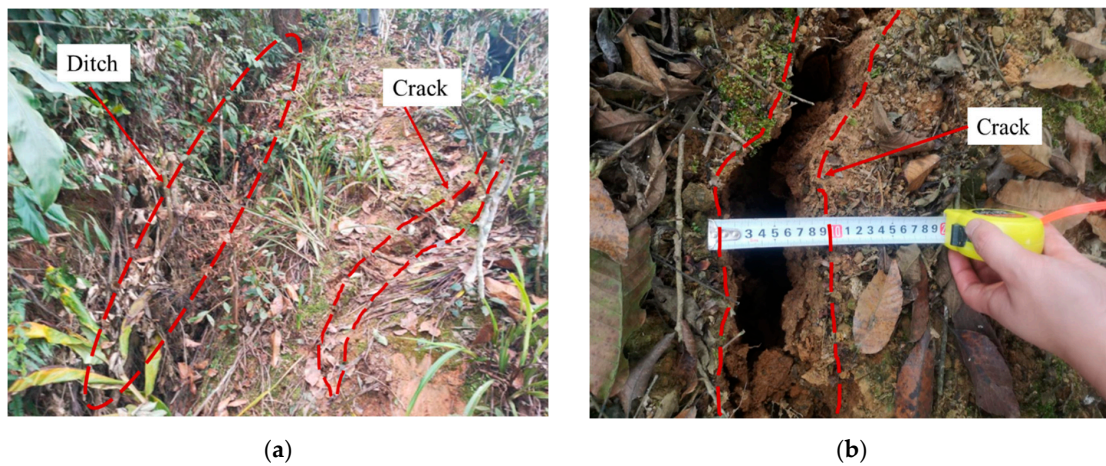


Figure 7. Deformation and crack diagram of the slope at the rear edge of the tunnel. (a) Slope of the rear edge and (b) the maximum deformation crack.



Figure 8. Cracking diagram of the lining of the right hole of the tunnel: (a) Peeling phenomenon of the primary support at the left vault of the right hole K142 + 115; (b) peeling of the initial branch at the left arch waist of the right hole K142 + 115.



Figure 9. Cracking diagram of the lining of the left hole of the tunnel: (a) Cracks in the arch waist on the right side of the left hole ZK142 + 130–140; (b) cracks in the arch wall on the right side of the left hole ZK142 + 130–140.

4. Numerical Simulation of the Underpass Landslide Tunnel

In this paper, a finite difference simulation model of the underpass landslide tunnel was established using FLAC3D by the detailed survey report. Considering the large variation in thickness of the powdered soil layer, the large workload and low accuracy of setting up a separate layer of material for simulation and the vegetation roots to enhance its strength, the powdered soil layer was combined into a strongly weathered layer for simulation. The model was divided into 138,580 blocks and 34,874 nodes, extending 266 m from north to south and 640 m from east to west, with an elevation difference of approximately 160 m between the top and bottom. The solid unit was used for the surrounding rock, the thin shell unit was used for the lining structure, and the boundary conditions were imposed as fixed at the bottom and as normal constraints on all the other faces. The dominant joint material was simulated over the entire joint, and the dominant joint yield was set at $-35^\circ/28^\circ$ with a joint spacing of 4 m. The rest of the material was simulated by using Moore Cullen. The physical and mechanical parameters of the surrounding rocks were adopted from the ground investigation report, and the parameters of each surrounding rock are shown in Table 1. The tunnel slope model is shown in Figure 10, where Soil-1 is a medium-weathered rock body (powdered clay), Soil-2 is a strongly weathered rock body, Soil-3 is a medium-weathered rock body, and Soil-planting is a plantation soil.

Table 1. Physical and mechanical parameters of the surrounding rock.

Surrounding Rock Level	Severe γ (kN/m ³)	Modulus of Deformation E (GPa)	Poisson's Ratio μ	Cohesion C (MPa)	Angle of Internal Friction φ (°)	Uniaxial Compressive Strength R_a (MPa)
Mesothermal rock masses	23.7	1.0	0.32	0.1	25	0.002
Strongly weathered rock masses	21.6	1.0	0.42	0.06	20	0.0012
Planting soil	22.5	0.05	0.3	0.05	20	0.0001
Moderately weathered rock masses (considering dominant joints)	N/A	N/A	N/A	0.03	25	0.0006
Strongly weathered rock masses (consider dominant joints)	N/A	N/A	N/A	0.012	20	0.0004

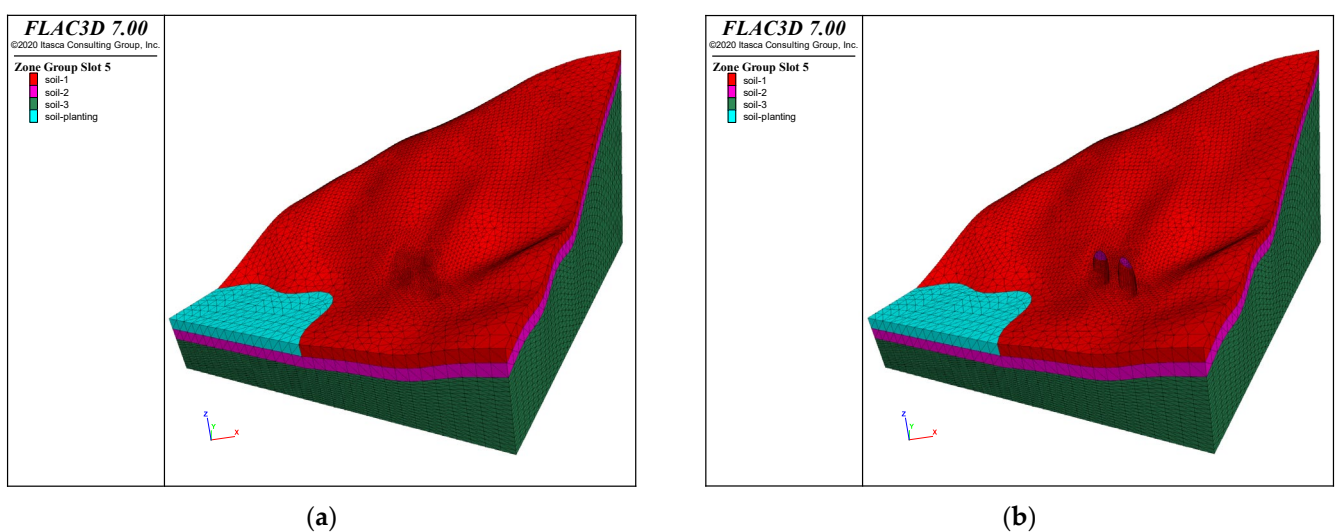
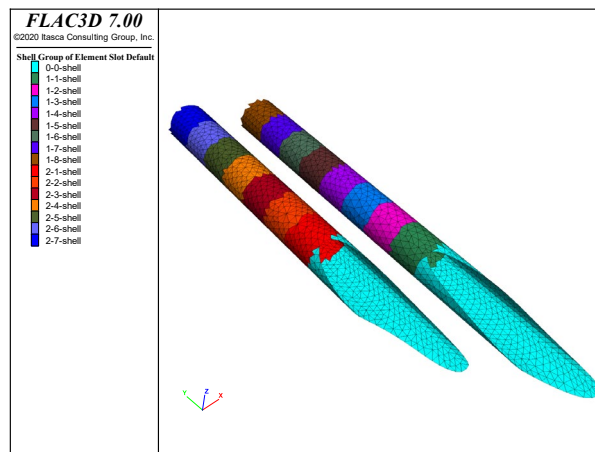


Figure 10. Cont.



(c)

Figure 10. Model drawing of the underpass landslide tunnel. (a) Slopes in their natural state and (b) slopes after tunnel excavation. (c) Lined structural body.

4.1. Simulation of Slope Stability in the Natural State

To investigate the effect of tunnel excavation on the stability of the slope, a static stability analysis of the slope in its natural state was carried out, and the stress region of the slope before tunnel excavation was calculated as shown in Figure 11, with the plastic damage zone as shown in Figure 12.

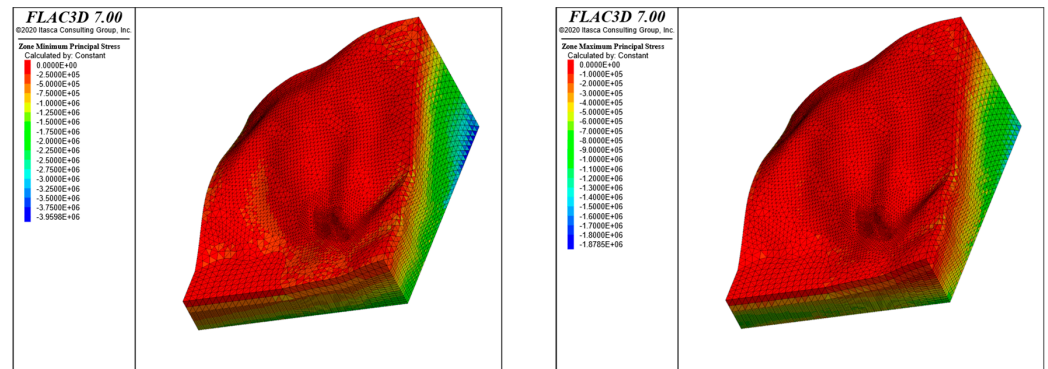


Figure 11. Stress zones.

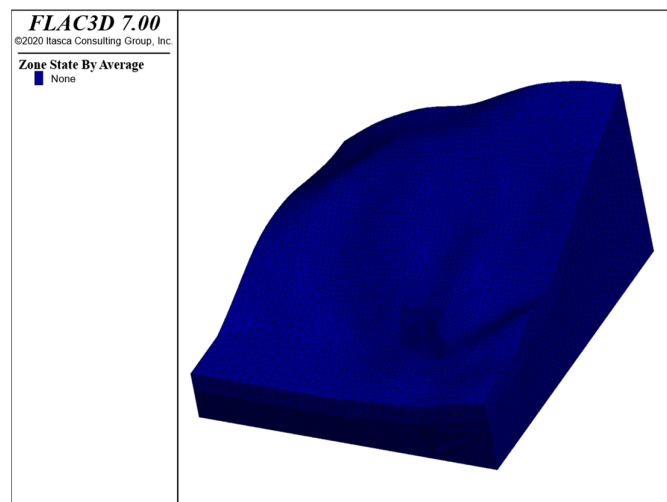


Figure 12. Plastic damage zone.

From Figures 11 and 12, it can be seen that the stress values of the slopes within the area of investigation were greater than 0, indicating that there was no tensile stress nor plastic damage zone on the slopes within the area of investigation. In addition, the presence of tree roots on the slope surface, which provided a relatively large anchorage force, indicated that there was no local landslide on the actual slopes and that the stability of the slopes before tunnel excavation was good.

4.2. Simulation of Slope Stability after Tunnel Excavation

To simplify the simulation process by ignoring the construction of the open tunnel and its impact on the slope, the entrance tunnel envelope was simulated with a simplified reinforcement treatment by increasing the cohesion value of the reinforcement area to 1 GPa, increasing the uniaxial tensile strength value of the reinforcement area to 0.1 GPa, leaving the friction angle unchanged, and using an increased strength parameter to remove the joints that existed throughout the reinforcement area. The tunnel excavation process was divided into three construction simulations: the first section of tunnel construction was based on an approximate simulation of the completion of the left and right tunnel sections up to 50 m; the second section of tunnel construction was based on the excavation of the left and right tunnels up to 60 m, with the right tunnel excavated and supported in time and the left tunnel not supported in time, causing the tunnel to collapse; and the third section of tunnel construction was based on the excavation of the left and right tunnels up to 88.4 m. The maximum stresses in the profile at key locations after excavation and construction of the three tunnel sections are shown in Tables 2–4, the plastic damage zone is shown in Figure 13, and the slope safety factor distribution is shown in Figure 14.

Table 2. Maximum stresses in each profile for the first section of tunnel construction.

Profile/Tunnel	Maximum Compressive Stress (MPa)	Maximum Tensile Stress (MPa)
Profile at 0 m/left line tunnel	2.01	0.24
Profile at 20 m/left line tunnel	3.36	0
Profile at 0 m/right line tunnel	2.65	0.18
Left line tunnel longitudinal section	1.79	0.14
Right line tunnel longitudinal section	1.61	0.18

Table 3. Maximum stresses in each profile for the second section of tunnel construction.

Profile/Tunnel	Maximum Compressive Stress (MPa)	Maximum Tensile Stress (MPa)
Profile at 0 m/left line tunnel	3.14	0.74
Profile at 20 m/left line tunnel	7.82	1.59
Profile at 0 m/right line tunnel	3.32	0.85
Profile at 60 m/left line tunnel	11.17	0.93
Profile at 40 m/right line tunnel	5.4	0.91
Left line tunnel longitudinal section	3.97	1.31
Right line tunnel longitudinal section	2.83	1.03

Table 4. Maximum stresses in each profile for the construction of the third tunnel section.

Profile/Tunnel	Maximum Compressive Stress (MPa)	Maximum Tensile Stress (MPa)
Profile at 0 m/left line tunnel	6.5	0.95
Profile at 20 m/left line tunnel	7.03	1.72
Profile at 0 m/right line tunnel	3.51	1.08
Profile at 60 m/left line tunnel	11.4	1.55
Profile at 40 m/right line tunnel	6.9	1.55
Profile at 70 m/left line tunnel	6.69	1.18
Profile at 60 m/right line tunnel	9.24	2.54
Profile at 80 m/left line tunnel	6.23	1.23
Profile at 70 m/right line tunnel	6.11	1.03
Profile at 88.4 m/left line tunnel	8.23	1.03
Profile at 78.4 m/right line tunnel	8.03	1.58
Left line tunnel longitudinal section	6.61	1.58
Right line tunnel longitudinal section	6.46	2.52

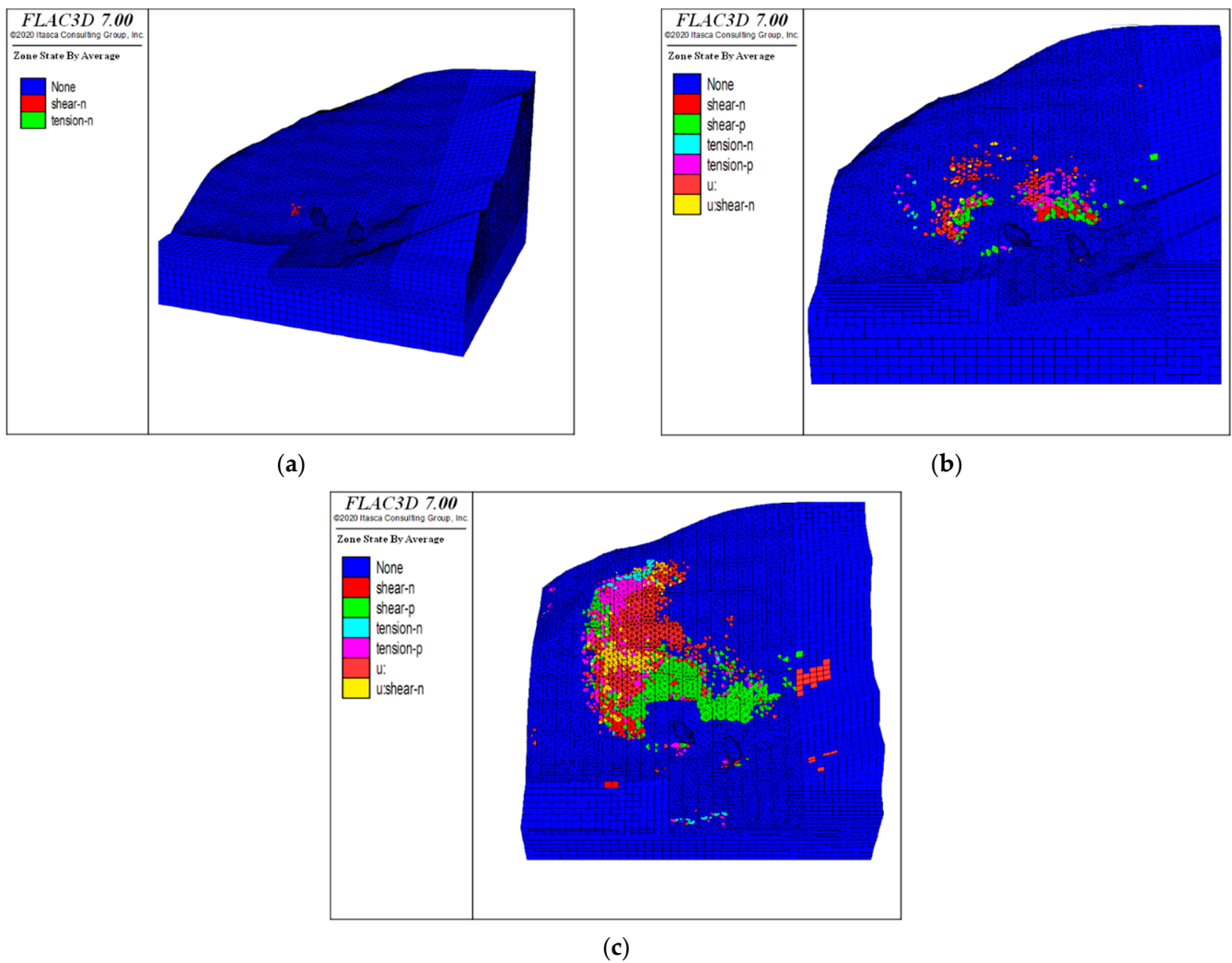


Figure 13. Zone of plastic damage: (a) First paragraph, (b) second paragraph, (c) third paragraph.

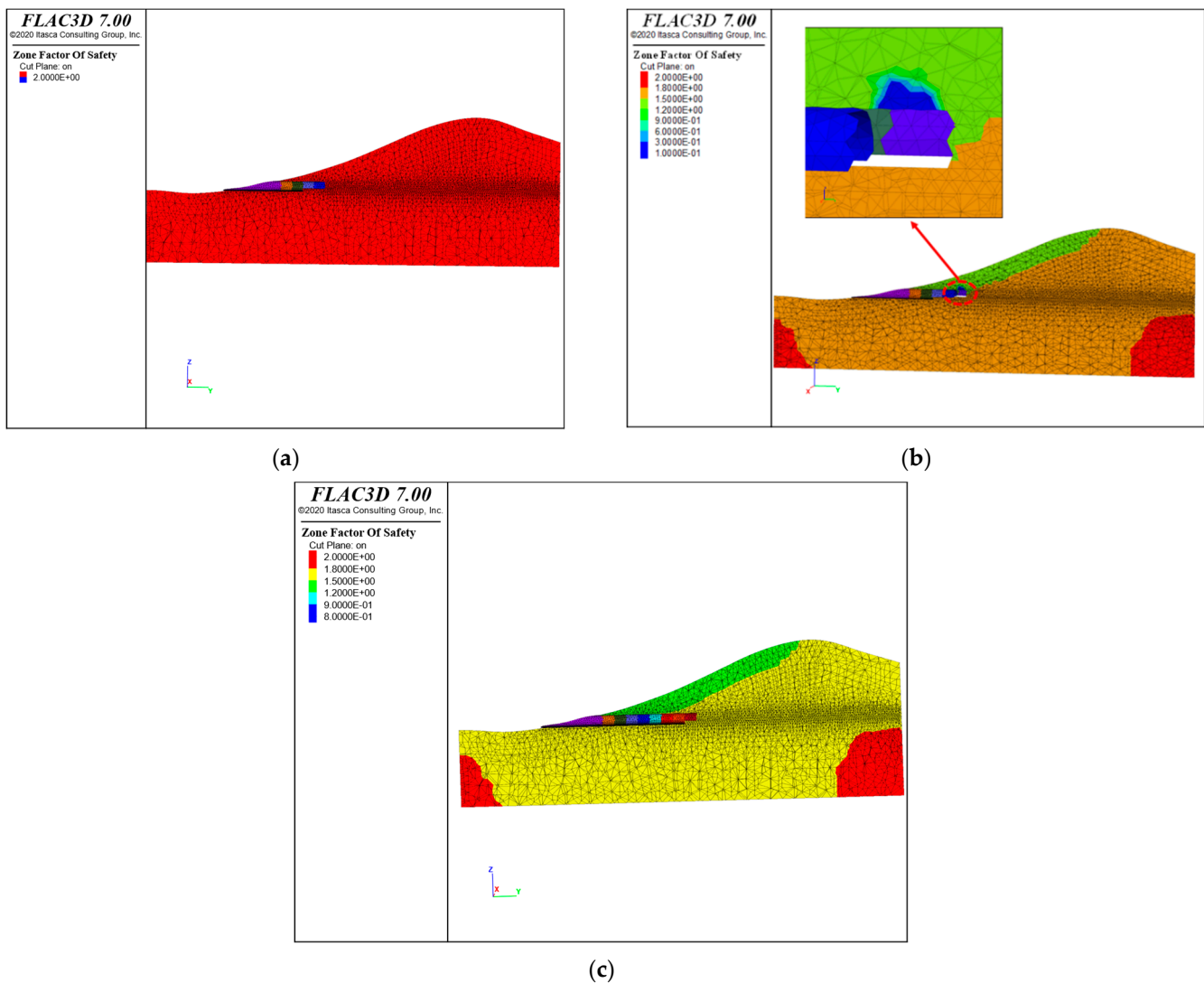


Figure 14. Distribution of slope safety factors: (a) First paragraph, (b) second paragraph, (c) third paragraph.

As can be seen from Tables 2–4, with the excavation of the tunnel, the stress on the tunnel lining structure by the side slope increased continuously, from a maximum pressure of 3.8 MPa to 11.4 MPa, indicating that the excavation caused the potential sliding surface of the side slope to slide down, and the sliding body generated thrust to act on the tunnel lining structure, resulting in increased stress.

After the completion of the first section of the tunnel construction, the tunnel lining range near the exit exhibited an obvious tensile stress zone, the maximum tensile stress being 0.24 MPa; the tensile stress was more likely to make the surrounding rock yield and damage, so the tunnel lining had the risk of generating tensile cracks. After the completion of the second section of tunnel construction, the range of tensile stress was increasing, the value of tensile stress at the same section increased, and the maximum tensile stress was as high as 1.59 MPa; at this time, the surrounding rock was very susceptible to yield and damage. The actual situation was that the tunnel collapsed, and outside the collapsed section of the left tunnel section, the tunnel lining produced tension cracks. After the third section of the tunnel construction was completed, the degree of stress concentration in the right tunnel increased in the same section, the degree of stress concentration in some sections of the left tunnel increased, and the degree of stress concentration in the sections affected by the tunnel collapse became smaller. The range of tensile stress tunnel sections was becoming increasingly larger, the maximum tensile stress value of the same tunnels in

the same section was increasing. The maximum tensile stress reading was found to be as high as 2.04 MPa, with the location being outside the collapsed section of the left tunnel; the actual situation was that the nearby uphill slopes produced tension cracks in a section of lining outside the collapsed section. The actual situation encompassed the location of the nearby elevation slope cracks, and, as can be seen from the calculation results, the actual situation was more consistent.

As can be seen in Figure 13, after the completion of the first section of tunnel construction, the plasticity zone existed in a very small range and was not connected to a piece; so, it can be seen that, at this time, the stability of the tunnel surrounding rock and slopes was good. After completion of the second section of tunneling, the plastic damage zones were created from the edge of the tunnel, reaching the surface and connecting into pieces, which could easily lead to surface cracks. The actual situation was that a section of approximately 25 m long cracks was created on the surface of the ground near the top of the collapsed section of the left tunnel. After the completion of the third tunnel section, the plastic damage zone grew from the surface above the right tunnel front and reached the surface above the left tunnel front and further expanded. The actual situation was that a 90 m long crack was created in the adjacent surface location, which showed that the calculation results were more consistent with the actual situation.

As can be seen from Figure 14, after the first section of tunnel construction, the slope safety coefficient was greater than 1, indicating that the slope was in a stable state. After the second section of tunnel construction, due to the failure of timely support after the excavation of the left line, the slope safety coefficient decreased, and the safety coefficient of a small range of slopes above the tunnel's unsupported place was less than 1. At this time, the tunnel was prone to cave-in damages, and the actual situation was that a small cave-in did occur here, with a volume of approximately 200 m³, forming a 6 m high collapse cavity at the top of the palm face. After the construction of the third section of the tunnel, the safety coefficient of some slopes was lower than 1. At this time, the surface was prone to tension cracks, and the actual situation was that a section of 90 m long cracks was produced in the similar surface position, which showed that the calculation results were more consistent with the actual situation.

For comparative analysis, numerical simulations were carried out for the construction of the tunnel without considering the presence of a left line tunnel collapse. The maximum stresses in the profile at key locations are shown in Table 5, the distribution of the plastic damage zone is shown in Figure 15, and the distribution of the side slope safety factor is shown in Figure 16.

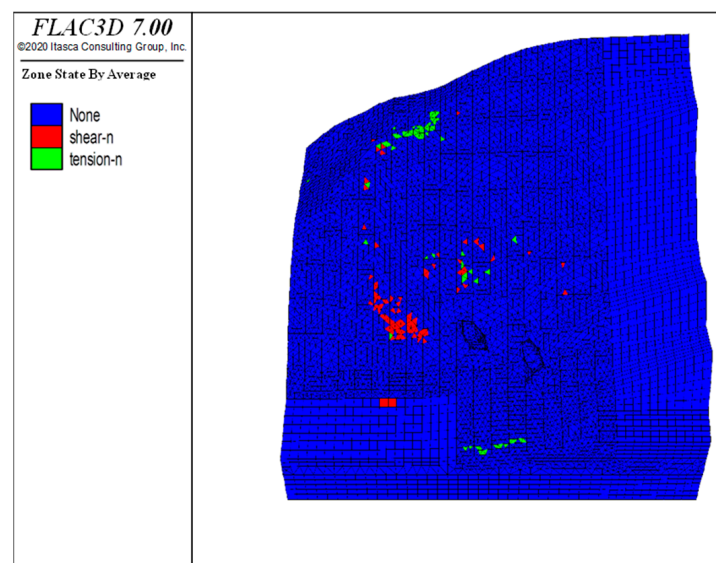
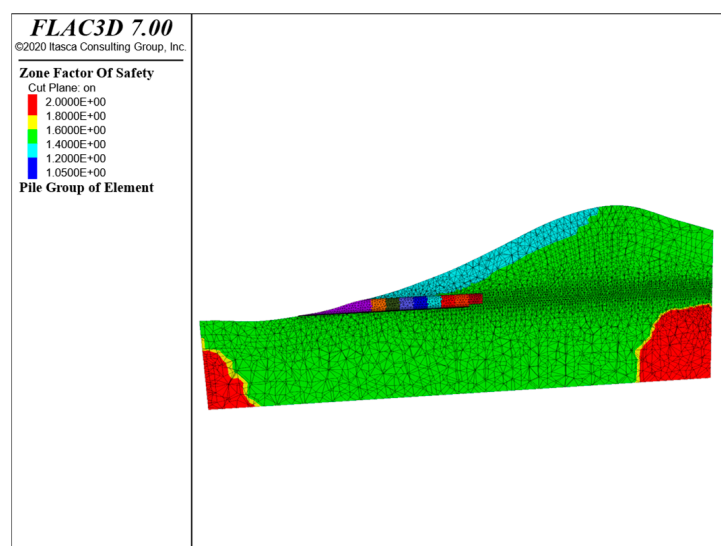


Figure 15. Distribution of plastic damage zones.

Table 5. Maximum stresses in each profile of the tunnel without collapse.

Profile/Tunnel	Maximum Compressive Stress (MPa)	Maximum Tensile Stress (MPa)
Profile at 0 m/left line tunnel	2.85	0.65
Profile at 20 m/left line tunnel	6.03	1.02
Profile at 0 m/right line tunnel	2.51	0.68
Profile at 60 m/left line tunnel	10.4	0.65
Profile at 40 m/right line tunnel	4.9	0.63
Profile at 70 m/left line tunnel	4.99	0.78
Profile at 60 m/right line tunnel	4.34	0.84
Profile at 80 m/left line tunnel	4.33	1.05
Profile at 70 m/right line tunnel	4.11	0.73
Profile at 88.4 m/left line tunnel	6.33	0.83
Profile at 78.4 m/right line tunnel	6.03	1.28
Left line tunnel longitudinal section	4.71	0.88
Right line tunnel longitudinal section	4.66	1.04

**Figure 16.** Distribution of slope safety factors.

As can be seen from Table 5 and Figures 15 and 16, compared with the simulation results of the tunnel collapse, the maximum stress value in the same section was significantly reduced, indicating that the tunnel collapse caused the potential sliding surface to slide down, and the slip body generated thrust to act on the tunnel lining structure body, resulting in an increased stress and a significant tunnel–slope interaction effect. The plastic damage zone near the left line tunnel did not appear to be connected to a patch, the plastic damage zone at the back edge of the mountain body, the relative increase in slope safety factor. This comparison shows that the collapse of the left tunnel was the main cause of a 25 m long crack in the ground surface near the top of the collapsed section of the left tunnel, and this hurt the ground surface at the back edge of the mountain, which showed a significant tunnel–slope interaction effect.

5. Analysis of the Interaction Damage Mechanism in Underpass Landslide Tunnels

According to the simulation calculation results and the results of the geological survey report to analyze the damage mechanism of the tunnel–slope interaction down through the landslide tunnel, we encountered weak surrounding rock, adverse geological bodies, tunnel import, and shallow export burial depth. After the excavation disturbance, a range of large elevation slope deformation damage was seen in the hole after the rock body

was broken (left line tunnel cracks), and not having timely support after the blasting excavation resulted in a potential sliding surface creep–slip action on the tunnel lining structure body. This resulted in tunnel convergence, sinking of the arch footings, and cracking of the lining. The presence of disintegrating mudstone caused the rock and soil on the slope to be less strong and more susceptible to deformation and damage; on the other hand, some of the disintegrating mudstone and hard rock, in the form of interlayer, was affected by weathering camp forces after excavation. The disintegrated mudstone and non-disintegrated rock produced differential weathering and formed a soft interlayer, as shown in Figure 17, which easily led to wedge-shaped sliding damage of the elevation slope and was not conducive to the stability of the debris rock elevation slope.

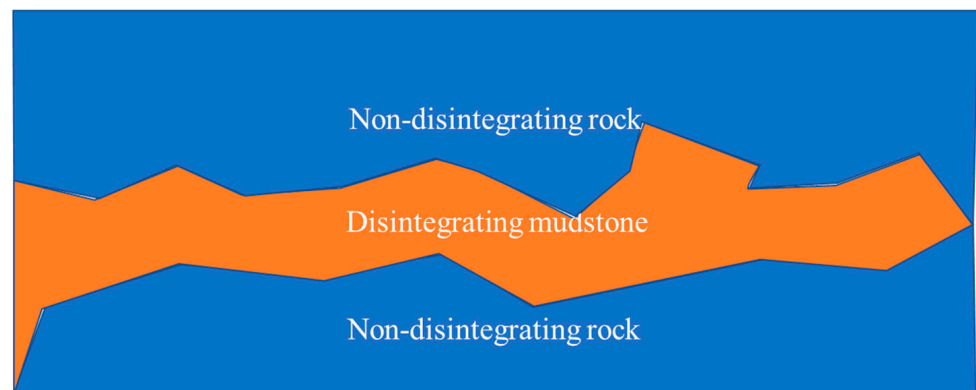


Figure 17. Form diagram of weak interlayer.

The interaction between tunnel damage and slope instability was magnified by the rheological nature of the mudstone contained in the tunnel envelope. When the tunnel was excavated to 50 m, the left tunnel collapsed, and a cavity was formed at the top of the collapsed cavity, resulting in some unloading, which led to the potential sliding surface of the elevation slope sliding down. The sliding stresses generated by the slope sliding down were applied back to the tunnel, further increasing the stresses in the lining structure and at the top of the cavity slope. The excavation at the foot of the cavern caused a relaxation of the lower structural stresses, which eventually led to the cracking of the lining structure and the cavern opening, with the cracking damage pattern as shown in Figure 18.

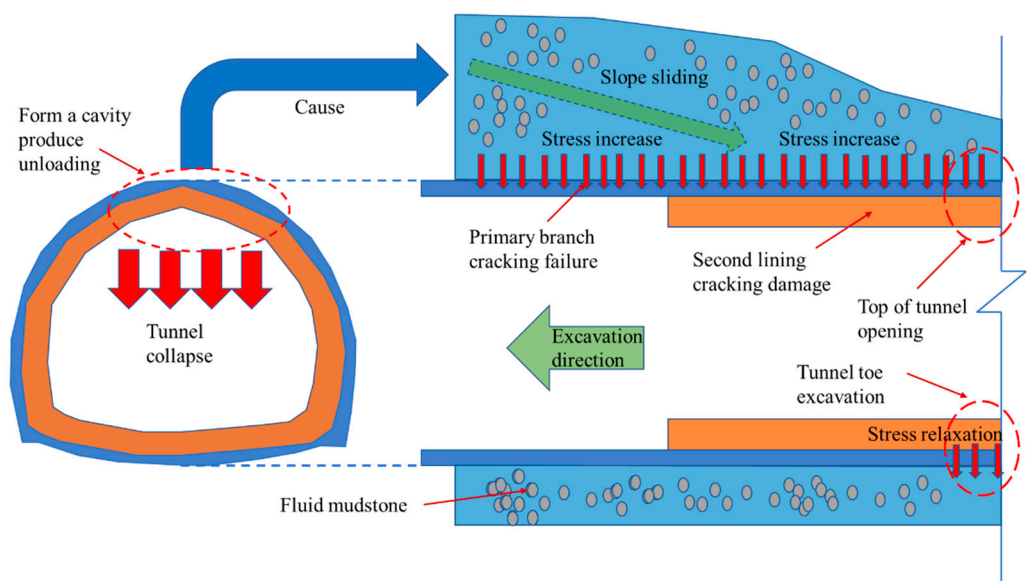


Figure 18. Failure mode diagram of lining structure.

6. On-Site Monitoring and Measurement

To grasp accurately the tunnel slope cracking deformation situation and predict the future deformation trend, tracking measurements were carried out at the location of the tunnel slope cracks. Sections K142 + 025, K142 + 028, and K142 + 034 were selected for horizontal and settlement deformation and displacement monitoring, and the relevant displacement–time and rate–time curves were obtained, as shown in Figures 19 and 20.

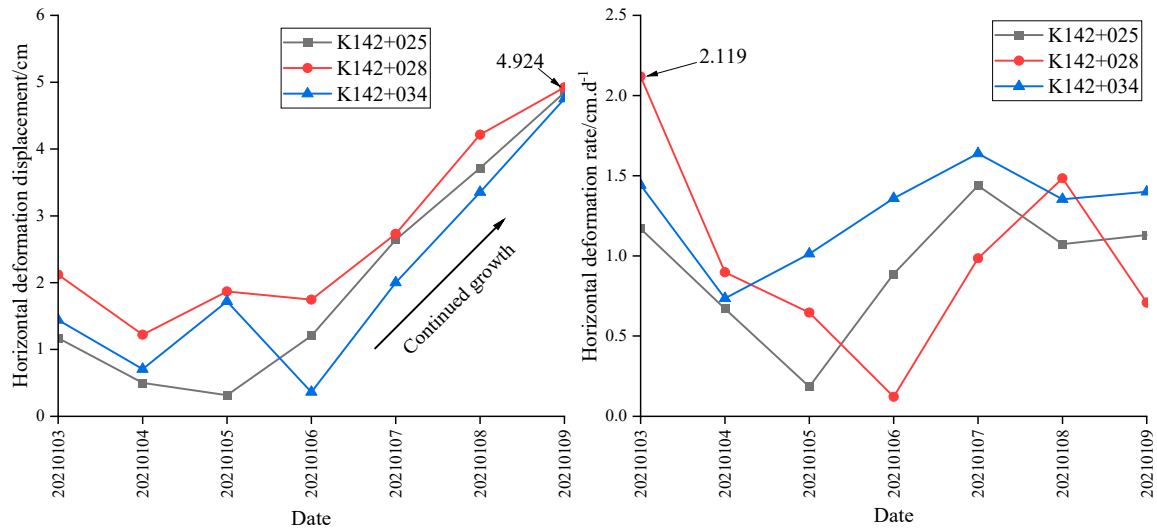


Figure 19. Horizontal monitoring map of the slope section.

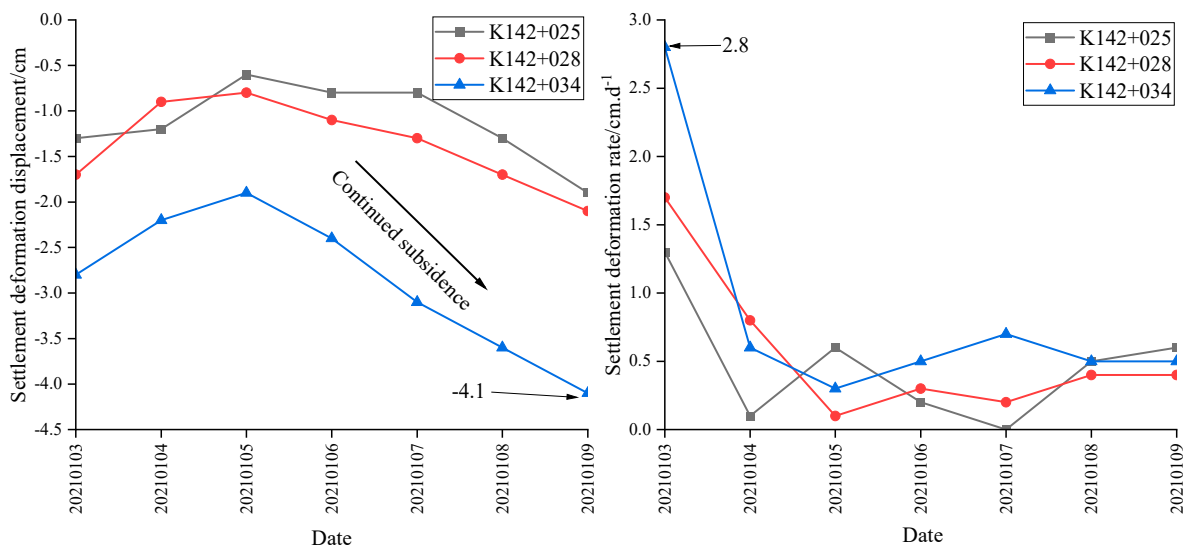


Figure 20. The subsidence monitoring map of the slope section.

From the deformation monitoring results shown in Figures 19 and 20, it can be seen that the horizontal deformation displacement of each section monitoring point showed a rising trend; the maximum horizontal deformation displacement value was 4.924 cm, and the horizontal deformation displacement was large, indicating that the stability of this section of the slope body was poor. The horizontal deformation rate was greater than 0 cm.d^{-1} , the maximum deformation rate was 2.119 cm.d^{-1} , and the overall deformation was 1 cm.d^{-1} , which indicated that the horizontal deformation of the slope would continue to increase.

The settlement deformation displacement of each section monitoring point showed a continuous sinking trend, the maximum settlement displacement value was -4.1 cm , and the sinking displacement value was large, indicating that the stability of this section of the slope was poor. The settlement deformation rate was greater than 0 cm.d^{-1} , the

maximum deformation rate was 2.8 cm.d^{-1} , and the overall fluctuation in the upper and lower sections was 0.5 cm.d^{-1} , which indicated that the amount of slope settlement would continue to increase.

In summary, the monitoring and measurement results showed that the horizontal deformation displacement and settlement deformation displacement of this section of the tunnel slope was increasing, indicating that the stability of this section of the slope body was poor and prone to instability, which would require emergency treatment measures and a permanent treatment plan to prevent further instability of the tunnel slope, resulting in serious consequences.

7. Disposal Options

The combination of geological investigation and simulation results showed that, except for the tunnel section in the strongly weathered rock layer, the landslide surface did not pass through the tunnel, the tunnel stress gradually increased without sudden changes, and the tunnel stress gradually increased due to the tunnel excavation, the rheological deformation of the rock body, and the collapse of the left line. Thus, the tunnel stress increase was normal and controllable, and by using the normal tunnel structural reinforcement measures as well as tunnel monitoring and control, the tunnel stability control requirements could be met. From the shallowness of the sliding body, it is clear that the sliding body was small, the sliding force was small, the sliding surface of the 3D landslide had not yet formed, the sliding body had residual slip resistance available, and the sliding body was stable according to Pan's law. Therefore, it is only necessary to take general reinforcement disposal measures for the areas where plastic zones may appear.

7.1. Numerical Simulation of Treatment Measures

This study simulated the treatment of tunnel slopes in FLAC3D to guide the actual reinforcement and treatment on site. The simulated solution to meet the slope stability control requirements consisted of slurry reinforcement, interception and drainage, surface grassing, toe counter-pressure, and anti-slip piles for areas where plastic zones may occur. The treated tunnel slope should meet the requirements of the Technical Specification for Construction Slope Engineering [42], which requires a permanent slope safety factor of more than 1.25.

As can be seen from Figure 21, the minimum safety factor after the reinforcement solution was 1.375, which was greater than the code requirement of 1.25. The slope of the tunnel after treatment met the stability requirements, and the treatment solution was feasible.

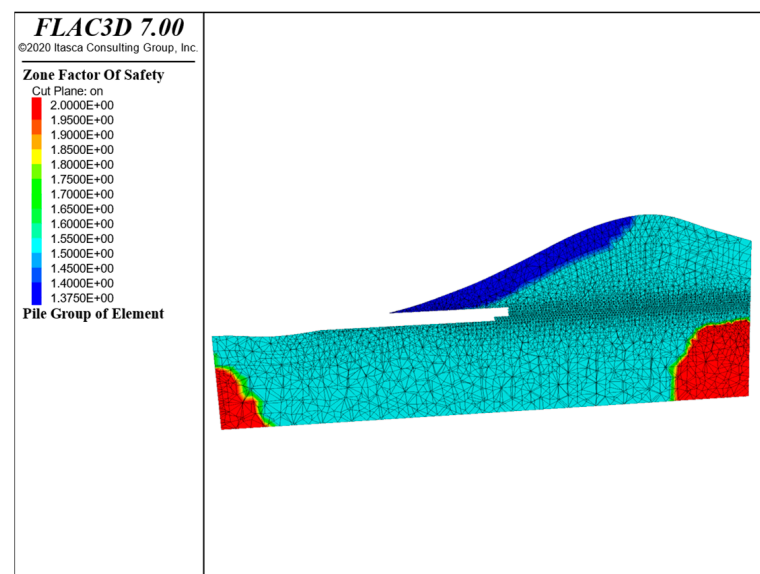


Figure 21. Distribution of safety factors of the treated tunnel slopes.

7.2. Practical Treatment Measures on Site

Combining the simulation results and the actual site conditions, we propose to adopt a comprehensive treatment plan of “tunnel cave-in rescue + tunnel slope treatment”.

7.3. Emergency Measures in Tunnel Caverns

Rescue measures: Stop tunnel palm face boring and use A8 reinforcement mesh and 10 cm thick C25 shotcrete to seal the palm face. To ensure that the initial support cracking and spalling of the tunnel was serious in the ZK142 + 120 to ZK142 + 140 section of the left cavern and the K142 + 100 to K142 + 120 section of the right cavern, the reinstatement arch was added to strengthen the support system, using I18 I-beams with a spacing of 80 cm. After the erection of the re-arch in section K142 + 120 was completed, backfilling was carried out in sections ZK142 + 110 to ZK142 + 150 in the left cavern and section of K142 + 090 to K142 + 130 in the right cavern using gravel or cavern slag, with the top surface of the backfilling elevated above the design height of 5 m. The backfilling surface was then leveled and, finally, 50 cm thick C25 plain concrete was poured on the top surface.

Structural strengthening measures: According to the surrounding rock conditions revealed in the cave and the numerical simulation results, the structural strengthening treatment was carried out, with the measures as follows:

- (1) The lining type of section ZK142 + 070~080 and section ZK142 + 030~040 of the left cave was adjusted from Sd4-b to Sd4-a for strengthening treatment.
- (2) The concrete standard of the lining of section ZK142 + 120~140 of the left cave and section K142 + 100~120 of the right cave was upgraded from C35 to C40, and the lining of section ZK142 + 130~140 of the left cave was changed from XSd5-a to XSd5-c for strengthening treatment.
- (3) The lining type of section K142 + 000 to K142 + 030 of the right cave was adjusted from Sd4-b to Sd5-b, and I-beams were added to the elevation arch of section K142 + 030 to K142 + 070 to close the initial support into a ring to improve the integrity of the initial support and strengthen the locking foot of this section.

7.4. Tunnel Slope Treatment

The treatment measures for the underpass landslide tunnel mainly included backfilling and backpressure, application of anti-slip piles, surface grouting, drainage treatment, and grass planting. The design of the treatment is shown in Figure 22.

- (1) Anti-slip piles: At a 880 m elevation, four square anti-slip piles with a length of 15 m (potential sliding surface depth of approximately 10 m), a pile cross section of 2 m × 4 m, and a pile spacing of 6 m were added to the back edge of the mountain; two square anti-slip piles with a length of 15 m (potential sliding surface depth of approximately 8 m), a pile cross section of 2 m × 4 m, and a pile spacing of 6 m were added to the right side of the left cavern.
- (2) Surface grouting: The length of grouting of the disturbed area caused by the collapse of the left tunnel at ZK142 + 140 was from mileage ZK142 + 120 to 130 on the left line and from mileage K142 + 112 to 120 on the right line. The width of grouting was from 30 m outside the outline of the left tunnel to 10 m outside the outline of the right tunnel, and the accumulated grouting area was approximately 600 m². The grouting material was P.O.42.5 cement net slurry, cement slurry with a water–cement ratio of (0.6–0.8):1, the initial pressure of grouting was 0.5–1.0 MPa, and the final pressure was 1.0 MPa.

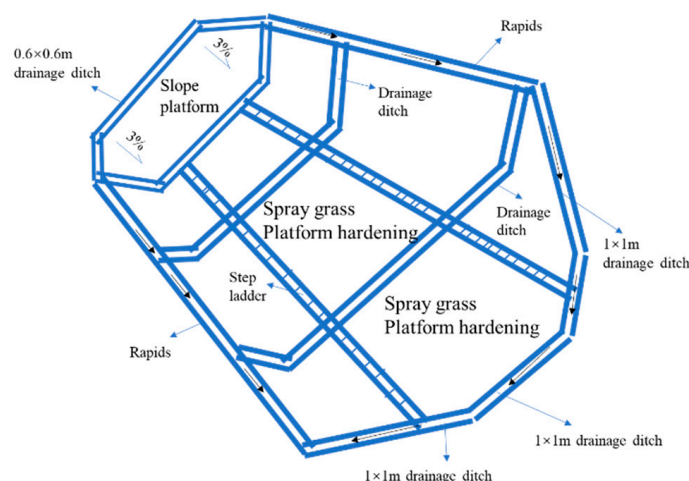


Figure 22. Design drawing of anti-pressure body treatment.

8. Conclusions

In this paper, a tunnel collapse occurred during the excavation of a subway landslide tunnel in southwest China, causing subsequent slope instability and lining cracking (the type of surrounding rock of this tunnel is widely found in southwest China and is representative). The analysis focused on the damage mechanism of the interaction between the tunnel collapse and the slope instability through an analysis of the damage mode using simulation as a reference. Combined with the actual situation on site, the targeted treatment plan of “tunnel cave-in rescue + tunnel slope treatment” was proposed, and the following conclusions were obtained:

- (1) The interaction effect between the tunnel collapse and the slope instability, as well as the fact that the large amount of mudstone commonly contained in the surrounding rock of this tunnel is rheological, can amplify the interaction effect on the tunnel slopes and lead to greater damage.
- (2) Mechanisms of interaction in underpass landslide tunnels: During the excavation process of the tunnel beneath the landslide, a weak sandwich geology was encountered, which resulted in the collapse of the left line tunnel. This collapse created an unloading effect, causing stress concentration on the elevation slope near the left line. A small potential sliding surface slippage occurred within a limited range, accompanied by a surface crack measuring approximately 25 m in length. The sliding force exerted on the elevation slope affected the tunnel, increasing the stress on the tunnel lining. As the excavation progressed, the stress on the elevation slope surged, causing the potential sliding surface slippage range to expand. A large crack, 2–10 cm in width and 91 m in length, appeared on the ground surface. The sliding force exerted on the elevation slope continued to affect the tunnel, resulting in damage and cracking of the lining.
- (3) This study adopted the comprehensive treatment plan of “tunnel cave-in rescue + tunnel slope treatment”, where tunnel cave-in includes stopping excavation, shotcrete reinforcement, re-arching, backfill and backpressure, reinforcing the structure, and tunnel slope includes backfill and backpressure, anti-slip piles, surface grouting, drainage, and grass planting. This plan has strong pertinence and effectiveness and solves the problem of tunnel cavity fundamentally and ensures the smooth excavation of the tunnel as well as the safety and stability of the tunnel slope.

Author Contributions: Writing—original manuscript preparation, W.Z.; software, X.X.; writing—review and editing, X.L.; research, S.L. All authors have read and agreed to the published version of the manuscript.

Funding: This research received no external funding.

Institutional Review Board Statement: Not applicable.

Informed Consent Statement: Written informed consent has been obtained from the patient(s) to publish this paper.

Data Availability Statement: The data used to support the findings of this study are available from the corresponding author upon request.

Conflicts of Interest: The authors declare that they have no conflicts of interest.

References

1. Zhong, T.; Ma, Q. Numerical analysis and research of entrance slope of shallow buried karst tunnel. In *IOP Conference Series: Earth and Environmental Science*; IOP Publishing: Bristol, UK, 2020; Volume 455, p. 12176.
2. Ruggeri, P.; Fruzzetti, V.M.E.; Vita, A.; Paternesi, A.; Scarpelli, G.; Segato, D. Deep-seated landslide triggered by tunnel excavation. In *Landslides and Engineered Slopes. Experience, Theory and Practice*; CRC Press: Boca Raton, FL, USA, 2018; pp. 1759–1766.
3. Wang, Z.; Yang, J.; Zhang, T.; Yao, C.; Zhang, X.; Gu, P. PPV and Frequency Characteristics of Tunnel Blast-Induced Vibrations on Tunnel Surfaces and Tunnel Entrance Slope Faces. *Shock. Vib.* **2021**, *2021*, 5527115. [[CrossRef](#)]
4. Lee, K.D.; Jung, U.Y.; Lee, J.D. A Case Study of Colluvium Slope Failure On Tunnel Entrance. *J. Korean Soc. Hazard Mitig.* **2015**, *15*, 345–351. [[CrossRef](#)]
5. Song, Y.S.; Yun, J.M. Analysis of the stability and behavior of a calcareous rock slope during construction of a tunnel entrance. *J. Eng. Geol.* **2013**, *23*, 283–292. [[CrossRef](#)]
6. Wang, Z.F.; He, S.M.; Liu, H.D.; Li, D.D. Formation mechanism and risk assessment of unstable rock mass at the Yumenkou tunnel entrance, Shanxi province, China. *Bull. Eng. Geol. Environ.* **2021**, *80*, 1433–1448. [[CrossRef](#)]
7. Song, D.; Chen, J.; Cai, J. Deformation monitoring of rock slope with weak bedding structural plane subject to tunnel excavation. *Arab. J. Geosci.* **2018**, *11*, 251. [[CrossRef](#)]
8. Weng, X.; Sun, Y.; Yan, B.; Niu, H.; Lin, R.; Zhou, S. Centrifuge testing and numerical modeling of tunnel face stability considering longitudinal slope angle and steady state seepage in soft clay. *Tunn. Undergr. Space Technol.* **2020**, *101*, 103406. [[CrossRef](#)]
9. Mahmood, K.; Kim, J.M.; Khan, H.; Safdar, M.; Khan, U. The probabilistic stability analysis of saturated-unsaturated MH and CL soil slope with rainfall infiltration. *KSCE J. Civ. Eng.* **2018**, *22*, 1742–1749. [[CrossRef](#)]
10. Lin, H.; Zhong, W. Influence of rainfall intensity and its pattern on the stability of unsaturated soil slope. *Geotech. Geol. Eng.* **2019**, *37*, 615–623. [[CrossRef](#)]
11. Fan, S.Y.; Song, Z.P.; Zhang, Y.W.; Liu, N.F. Case study of the effect of rainfall infiltration on a tunnel underlying the roadbed slope with weak inter-layer. *KSCE J. Civ. Eng.* **2020**, *24*, 1607–1619. [[CrossRef](#)]
12. Ren, Y.; Li, T.; Lai, L. Centrifugal shaking table test on dynamic response characteristics of tunnel entrance slope in strong earthquake area. *Rock Soil Mech.* **2020**, *41*, 1605.
13. Niu, J.; Jiang, X.; Yang, H.; Wang, F. Seismic response characteristics of a rock slope with small spacing tunnel using a large-scale shaking table. *Geotech. Geol. Eng.* **2018**, *36*, 2707–2723. [[CrossRef](#)]
14. Xin, C.L.; Wang, Z.Z.; Zhou, J.M.; Gao, B. Shaking table tests on seismic behavior of polypropylene fiber reinforced concrete tunnel lining. *Tunn. Undergr. Space Technol.* **2019**, *88*, 1–15. [[CrossRef](#)]
15. Chen, C.; Nie, Y.; Zhang, Y.; Lei, P.; Fan, C.; Wang, Z. Experimental investigation on the influence of ramp slope on fire behaviors in a bifurcated tunnel. *Tunn. Undergr. Space Technol.* **2020**, *104*, 103522. [[CrossRef](#)]
16. Kim, J.T.; Hong, K.B.; Ryou, H.S. Numerical analysis on the effect of the tunnel slope on the plug-holing phenomena. *Energies* **2018**, *12*, 59. [[CrossRef](#)]
17. Kim, J.T.; Ryou, H.S. Experimental Study on Effect of Tunnel Slope on Heat Release Rate with Heat Feedback Mechanism. *Fire Technol.* **2021**, *57*, 2661–2681. [[CrossRef](#)]
18. Du, X.W.; Gao, Y.T. On the stability and control technology of the side slope of the tunnel entrance. *Appl. Mech. Mater.* **2014**, *488*, 737–740. [[CrossRef](#)]
19. Song, D.; Liu, X.; Chen, Z.; Chen, J.; Cai, J. Influence of tunnel excavation on the stability of a bedded rock slope: A case study on the mountainous area in southern Anhui, China. *KSCE J. Civ. Eng.* **2021**, *25*, 114–123. [[CrossRef](#)]
20. Chiu, Y.C.; Lee, C.H.; Wang, T.T. Lining crack evolution of an operational tunnel influenced by slope instability. *Tunn. Undergr. Space Technol.* **2017**, *65*, 167–178. [[CrossRef](#)]
21. Ren, B.; Shen, Y.; Zhao, T.; Li, X. Deformation monitoring and remote analysis of ultra-deep underground space excavation. *Undergr. Space* **2023**, *8*, 30–44. [[CrossRef](#)]
22. Shen, Y.; Ling, J.; Lu, X.; Zhang, Y.; Yan, Z. Steel wire prestress analysis of large section jacking prestressed concrete cylinder pipe (JPCCP): Site experiment and numerical investigation. *Thin-Walled Struct.* **2023**, *184*, 110420. [[CrossRef](#)]
23. Jiang, X.; Zhang, X.; Wang, S.; Bai, Y.; Huang, B. Case study of the largest concrete earth pressure balance pipe-jacking project in the world. *Transp. Res. Rec.* **2022**, *2676*, 92–105. [[CrossRef](#)]
24. Causse, L.; Cojean, R.; Fleurisson, J.A. Interaction between tunnel and unstable slope—Influence of time-dependent behavior of a tunnel excavation in a deep-seated gravitational slope deformation. *Tunn. Undergr. Space Technol.* **2015**, *50*, 270–281. [[CrossRef](#)]
25. Lu, L.; Liang, S.; Luo, S.; Li, J.; Zhang, B.; Hu, H. Optimization of the construction technology of shallow-buried tunnel entrance constructed in residual slope accumulation of gravelly soil. *Geotech. Geol. Eng.* **2018**, *36*, 2391–2401. [[CrossRef](#)]

26. Koçkar, M.K.; Akgün, H. Methodology for tunnel and portal support design in mixed limestone, schist and phyllite conditions: A case study in Turkey. *Int. J. Rock Mech. Min. Sci.* **2003**, *40*, 173–196. [[CrossRef](#)]
27. Kong, F.; Lu, D.; Du, X.; Shen, C. Displacement analytical prediction of shallow tunnel based on unified displacement function under slope boundary. *Int. J. Numer. Anal. Methods Geomech.* **2019**, *43*, 183–211. [[CrossRef](#)]
28. Kaya, A.; Akgün, A.; Karaman, K.; Bulut, F. Understanding the mechanism of slope failure on a nearby highway tunnel route by different slope stability analysis methods: A case from NE Turkey. *Bull. Eng. Geol. Environ.* **2016**, *75*, 945–958. [[CrossRef](#)]
29. Lei, M.F.; Lin, D.Y.; Yang, W.C.; Shi, C.H.; Peng, L.M.; Huang, J. Model test to investigate failure mechanism and loading characteristics of shallow-bias tunnels with small clear distance. *J. Cent. S. Univ.* **2016**, *23*, 3312–3321. [[CrossRef](#)]
30. Hu, Z.; Shen, J.; Wang, Y.; Guo, T.; Liu, Z.; Gao, X. Cracking characteristics and mechanism of entrance section in asymmetrically-load tunnel with bedded rock mass: A case study of a highway tunnel in southwest China. *Eng. Fail. Anal.* **2021**, *122*, 105221. [[CrossRef](#)]
31. Deng, X.; Xu, T.; Wang, R. Risk evaluation model of highway tunnel portal construction based on BP fuzzy neural network. *Comput. Intell. Neurosci.* **2018**, *2018*, 8547313. [[CrossRef](#)]
32. Sun, T.; Yue, Z.; Gao, B.; Li, Q.; Zhang, Y. Model test study on the dynamic response of the portal section of two parallel tunnels in a seismically active area. *Tunn. Undergr. Space Technol.* **2011**, *26*, 391–397. [[CrossRef](#)]
33. Zhao, J.; Lan, W.; Wang, G. Analysis of seismic Response and Slope Stability for Intake Tunnel Entrance of Hongyan River Nuclear Project. In *IOP Conference Series: Earth and Environmental Scienc*; IOP Publishing: Bristol, UK, 2019; Volume 304, p. 42047.
34. Wang, J.; Zeng, Y.; Xu, Y.; Feng, K. Analysis of the influence of tunnel portal section construction on slope stability. *GeoloGy Ecol. Landsc.* **2017**, *1*, 56–65. [[CrossRef](#)]
35. Chen, L.L.; Wang, Z.F.; Wang, Y.Q. Failure analysis and treatments of tunnel entrance collapse due to sustained rainfall: A case study. *Water* **2022**, *14*, 2486. [[CrossRef](#)]
36. Hou, T.; Duan, X.; Liu, H. Study on stability of exit slope of Chenjiapo tunnel under condition of long-term rainfall. *Environ. Earth Sci.* **2021**, *80*, 590. [[CrossRef](#)]
37. Wu, H. Research on the Deformation Mechanism and Control Technology of Tunnel-Landslide System. *Chin. J. Rock Mech. Eng.* **2012**, *31*, 3632–3642. (In Chinese)
38. Tao, Z.; Zhang, Q.; Yang, X.J.; Zhao, F.; Cao, S.; Li, S. Experimental study on physical modeling of the effect of underpass tunnel excavation on the stability of loose-packed slopes. *J. Coal* **2022**, *47*, 61–76. (In Chinese)
39. Shao, Z.; Cui, F.; Li, C.; Ding, B. Research on factors influencing slope stability and treatment technology of powder clay tunnels. *J. Railw. Sci. Eng.* **2020**, *17*, 2055–2064. (In Chinese)
40. Ma, H.; Wu, H.; Yang, T. *Research on Deformation Mechanism and Control Technology of Landslide System in Land Traffic Tunnel*; Science Press: Beijing, China, 2020; pp. 118–128. (In Chinese)
41. Wu, H.G.; Zhao, J.; Li, Y.R.; Chen, S.Y. Research on additional load calculation method for tunnel underpassing landslide. *J. Rock Mech. Eng.* **2018**, *37*, 4375–4383.
42. GB 50330-2002; Technical Specifications for Construction Slope Works. China Construction Industry Press: Beijing, China, 2002. (In Chinese)

Disclaimer/Publisher’s Note: The statements, opinions and data contained in all publications are solely those of the individual author(s) and contributor(s) and not of MDPI and/or the editor(s). MDPI and/or the editor(s) disclaim responsibility for any injury to people or property resulting from any ideas, methods, instructions or products referred to in the content.